Effects of synthetic routes on structural, dielectric and electrical properties of CaCu$_3$Ti$_4$O$_{12}$ ceramics

Emna Souidi[1],* , Senda Saîd[1], Cécile Autret-lambert[2], Daniela Neacsa[2], and Adel Megriche[1]

[1] *Faculté des Sciences de Tunis, Laboratoire de Chimie Minérale Appliquée (LR19ES02), Université de Tunis el Manar, Campus Universitaire Farhat Hached, 2092 Tunis, Tunisia*

[2] *Parc de Grandmont, GREMAN, UMR 7341 CNRS, Universite Francois Rabelais, UFR Sciences et Techniques, 37200 Tours, France*

ABSTRACT

CaCu$_3$Ti$_4$O$_{12}$ (CCTO) ceramics was fabricated by solid,citrate,urea and glycine methods. The major goal is to assess the effects of synthesis techniques on the structural and electrical properties of the material. Independently of the synthesis method, X-ray diffraction XRD results confirmed presence of the cubic structure main phase with space group *Im* $\overline{3}$. The average grain size of the sample CCTO varied according to the synthesis process. The surface morphology of the composite sintered at 1100 °C for 12 h obtained by scanning electron microscopy analysis indicates the evolution of large and small grains with a bimodal distribution. A high dielectric constants ($\varepsilon' \sim 10^4$) accompanied fortunately by a lowering loss tangent ($\tan\delta < 0.1$) was measured at room temperature in the 10^2 Hz- 10^7 Hz frequency range in all ceramics. Ceramics elaborated by the citrate method show a very interesting dielectric response, namely a relatively high dielectric constant ε' (6.735×10^4 at 1 kHz) and a low dielectric loss $\tan\delta$ (0.07 at 1 kHz).In addition, the temperature stability of the dielectric constant also improved by solid, urea and glycine methods. The fits of impedance complex spectroscopy data, shows that the resistance of grain is lower than resistance of grain boundaries confirming the internal barrier layer capacitor model. This mechanism corresponds to the heterogeneous dielectric with semiconductor grains and insulating grain boundaries.

1 Introduction

The tremendous advancement in electronic materials technology has been constantly boosted towards an even more advanced miniaturization to improve their performances. Among the most active research areas, the improvement of dielectric properties of semi-conductors can be cited [1–3]. Thus, these research works aim to develop the dielectric material features that play a key role in industrial demand. Over the past decade, Copper Calcium Titanate (CCTO) is greatly important thanks to its dielectrics properties

such as a colossal dielectric constant ($\varepsilon_r > 10^4$) in a large temperature (40–400 K) and frequency [10^2–10^6 Hz] range [4, 5].

In addition to these excellent dielectric properties, CCTO is also characterized by an abnormally strong nonlinear current–voltage [6]. These excellent properties render this material mostly eye-catching for a broad range of applications, such as capacitor [7, 8], microwave devices antennas [9], and gas or humidity sensor [10, 11]. Also they can also be used for important devices such as automobiles and aircrafts [12].

Nevertheless, the greatest drawback of this CCTO material, limiting its use in capacitor applications [13, 14] is their high dielectric loss tangent (tanδ). Numerous investigations, either by substitution or by formation of composites, aim to control the evolution of this capital parameter. Unfortunately, the improvement of the dielectric loss values generally leads to a degradation of the dielectric constant.

There are several explanations for the mechanism of the giant dielectric properties of CCTO [15–17] such as internal domain, electrode polarization effect bimodal grain size, nanoscale barrier layer capacitance model (NBLC) [18, 19] and internal barrier layer capacitance IBLC [20, 21]. The latter is presented as the most acceptable theory, which is composed of semi conducting grains delimited by insulating grain boundaries [22]. This is why several researchers claim that the dielectric properties can be affected by several extrinsic factors such as microstructural, porosity and impurities [23].

From this model, ε_r of CTTO ceramics can be described with the following formula:

$$\varepsilon_r = \varepsilon_{gb} * \frac{d}{e}$$

where d is the mean grain size, e is the thickness of grain boundary and ε_{gb} is the ε_r of the insulating grain boundaries [24]. According to this formula, it can be noted that the dielectric constant and loss tangent values of CCTO are sensitive to the processing conditions, such as sintering time, sintering temperature and atmosphere, etc. [25, 26]. Several research groups have been working on the optimization of high-performance CCTO ceramics by different methods [27]. Basically, CCTO is prepared by solid state reaction [28, 29]. As an alternative to solid state process, wet methods have been

developed for the synthesis of CCTO such as sol–gel method [30], organic-precursor pyrolysis method [31], oxalate-coprecipitation method [32], semi-wet method [33], combustion employing glycine [34] and urea as fuels [35]. These techniques are interesting methods that can be used to improve the properties of CCTO ceramics. In his research, Laxman et al. have shown that a giant dielectric constant and a small loss tangent of ∼ 0.088 at 10 kHz are found in CCTO sample by semi wet route [36]. Pu Mao et al. have used sol gel method to synthetize CCTO powders witch present a high ε_r value (3 10^4 at 1 kHz) [37]. In addition, Thongbai et al. [38] used glycine as fuel to synthetize CCTO powders. Best values obtained are 10^4 –10^5 for the relative permittivity and 0.017–0.054 for low dielectric loss tanδ. Taking account the results int the literature, the aim of the paper is to investigate the properties of CCTO synthesized by different methods of synthesis, namely solid-state reaction, modified citrate method and solution by sol–gel route using urea and glycine separately.

2 Experimental

2.1 Solid state reaction

CCTO powder was prepared by solid state reaction. The precursor oxides of $CaCO_3$ (99%, Aldrich Chemical), TiO_2 (99.9%, Aldrich Chemical) and CuO (99.9%, Aldrich Chemical) were thoroughly mixed for 24 h using ZrO_2 balls in a suitable ethanol and then ground to fine powder in an agate mortar. The mixture powder was heated at temperatures varying from 800 to 1100 °C for 24 h in order to cause densification of the material, with intermediate manual grindings. The objective of this crushing was to obtain very fine grains and ensure better homogenization. Finally, the mixture was cold pressed into pellets and sintered at 1100 °C for 12 h.

2.2 Wet chemical

In this method, the mixing process was performed in solution state as nitrate solutions. It's interest allows to obtain powders with homogeneous chemical distribution, an excellent control of the composition. This technique involves the mixing of solutions of a metal precursor and an organic polyfunctional acid possessing at least one hydroxyl and one carboxylic

acid group such as citric acid, glycine, urea, tartaric and glycerol which results in complexation of the metal by the polycarboxylic acid.

Most of the combustion processes cited in the literature for the preparation of CCTO use citric acid, glycine, urea, egg, EDTA. These types of fuels offer an environment friendly fast and economic alternative for the preparation of such materials.

2.2.1 By glycine combustion method

In this technique, the precursors used for the preparation of catalysts were Ca (NO$_3$)$_2$·4H$_2$O, Cu (NO$_3$)$_2$·3H$_2$O, Aldrich Chemical, C$_{16}$H$_{28}$O$_6$Ti, and glycine (NH$_2$CH$_2$COOH, Aldrich Chemical) as the starting materials. The metal nitrates were dissolved in distilled water to obtain standard aqueous solutions of Ca^{2+}(aq), Cu^{2+}(aq). Stoichiometric amounts of C$_{16}$H$_{28}$O$_6$Ti were added to the solution with continuous stirring. In this route, glycine was used as a chelating agent for metal precursors: it can effectively complex a cation because of its carboxylic acid and amino groups. On the other hand, the glycine is probably most used as environmentally compatible in the combustion reaction [39, 40]. Indeed, the calculated amount of glycine equivalent to metal ions was added to the solution to form the complex. The aqueous solution of nitrates and glycine were homogenously mixed and then slowly heated at 50 °C to form viscous gel. The viscous gel was annealed at 350 °C for 30 min. During annealing, the gel was amplified into fluffy mass, which eventually broke into brittle flakes. Figure 1 shows the heat treatment of the CCTO powders obtained at different calcination temperatures 600 °C, 800 °C and 900 °C for 12 h respectively. Pellets were pressed and sintered at 1100 °C for 12 h in a muffle furnace.

2.2.2 By a urea combustion method

In this method, urea was used as fuel. Ca(NO$_3$)$_2$·4H$_2$O, Cu (NO$_3$)$_2$·3H$_2$O and C$_{16}$H$_{28}$O$_6$Ti were used as the starting raw materials. First, stoichiometric amounts of nitrate solutions and C$_{16}$H$_{28}$O$_6$Ti were dissolved in distilled water and stirred at room temperature for 30 min. Second, in another beaker, stoichiometric amount of NH$_2$CONH$_2$ was dissolved in distilled water. Then, the resulting mixture was heated on a hot plate under stirring at 70–80 °C to evaporate water and allow self-ignition until the
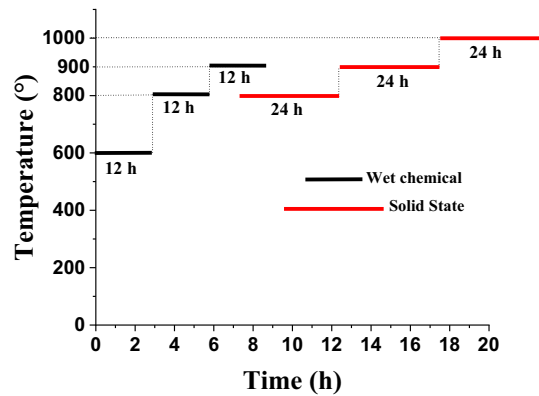

**Fig. 1** General thermal cycle for the wet chemical and solid-state methods

mixed solution was transformed into a viscous gel. The gel was annealed at 350 °C for 30 min. The obtained powder was grounded and calcined at different temperatures as shown in Fig. 1. Then pressed into pellets of 12 mm in diameter and 1 mm in thickness. The pellets were sintered in air at 1100 °C for 12 h.

2.2.3 Modified citrate method

This process synthesized by an organic gel-assisted citrate process consists in the gel formation by an auxiliary organic polymer in an aqueous nitrate solution in proper ratios [41–43]. In the first step, Ca (NO$_3$)$_2$·4H$_2$O, Cu (NO$_3$)$_2$·3H$_2$O and citrate titanium C$_{24}$H$_{20}$O$_{28}$Ti$_3$ were stoichiometrically calculated and mixed in the proper ratio by magnetic stirring. Cations were chelated by addition of a triammonium citrate solution with a suitable composition. The gel formation was obtained by addition of acrylamide and N, N-methylene-bis-acrylamide monomers, and azoisobutyronitrile (AIBN) catalyst to induce polymerization heating up to about 100 °C. The gel obtained at 500 °C was then calcined in a muffle furnace. The calcinations of resulting product oxide were carried out using a defined heating cycle as in Fig. 1.

2.2.4 Sintering

The resultant mixtures were ground into fine powders using a pestle and mortar, and cylindrical pellets were made using a hydraulic press. The pellets were sintered at 1100 °C for 12 h in air.
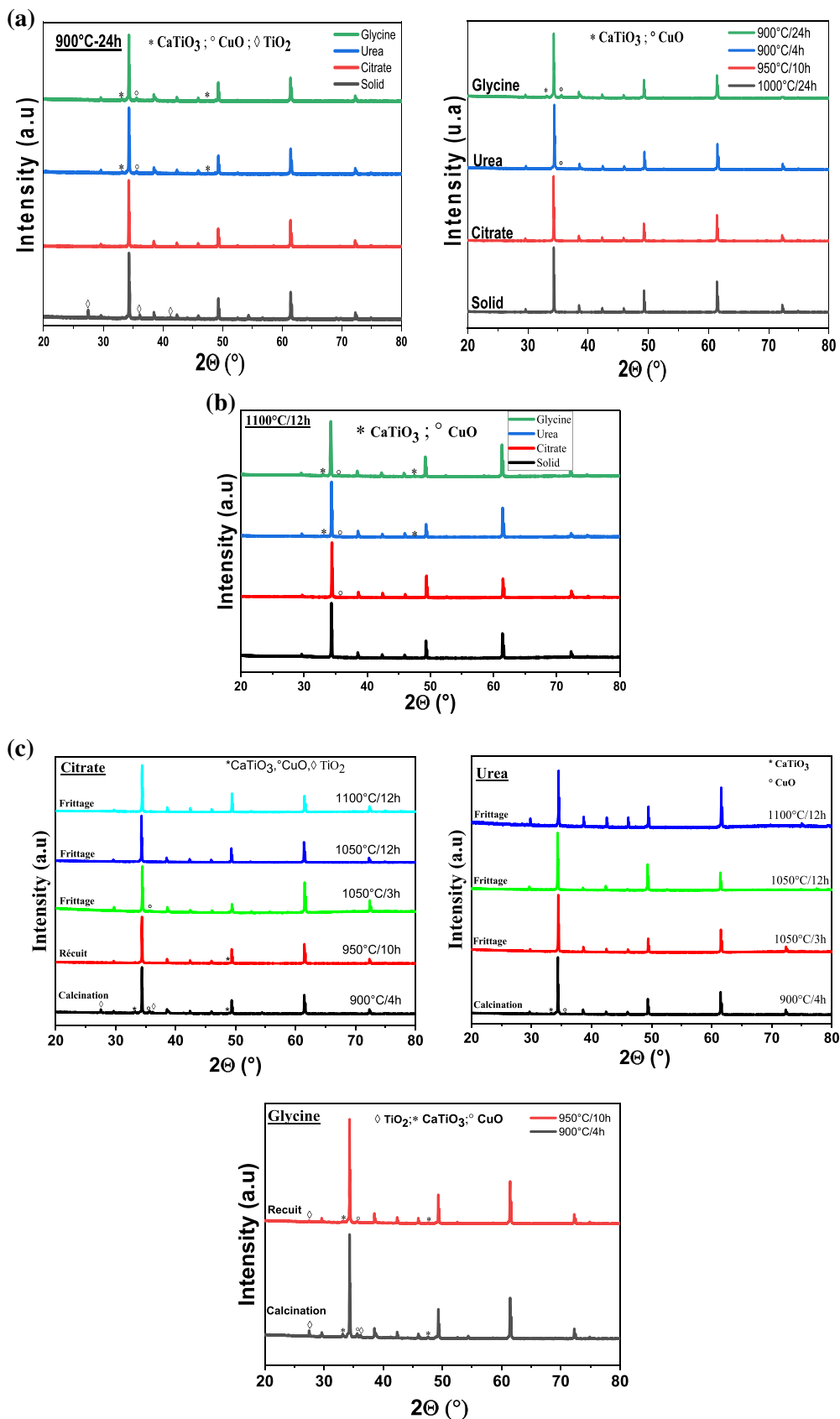
◄ **Fig. 2 a** X-ray diffraction patterns of CCTO powder calcined at different temperature. **b** X-ray powder diffraction patterns of CCTO compounds calcined at 900 °C-24 h and sintered at 1100°C12 hours. (stars in the figure indicate the peak due to phase with CaTiO₃ and CuO). **c** X-ray powder diffraction patterns of CCTO compounds synthesized by citrate, urea and glycine routes

3　Characterization

The obtained CCTO were characterized by X-ray diffraction (XRD) employing a D8 Bruker with CuKα radiation (λ = 1.540 Å) in the 2θ scan range of 10°–80°. The Rietveld refinement of the crystal structures was carried out with the Full Prof Software [44]. The microstructure and chemical composition of samples were investigated using scanning electron microscopes (SEM) MESU 1644 – HR JEOL. The Energy Dispersive X-ray Analyzer EDX was used for elemental analysis in the sintered samples of the above system. Before the dielectric measurements, the surfaces of all sintered ceramics were polished to obtain smooth surface. Samples were then coated with silver paste, and dried in air at 180 °C for 4 h. The pellets were characterized by dielectric spectroscopy using an Agilent 4294 A over a frequency range of 100 Hz up to 1 MHz at the room temperature.

4　Results and discussion

4.1　X-ray diffraction

Powders from differents synthesis methods were calcined at different times for the temperatures ranging from 900 °C to 1000 °C. Comparing the peaks of Fig. 2a with the published XRD patterns we find that all the major peaks of the of CCTO phase are present in our samples [45]. Supllementary,minor peaks belonging to CaTiO₃ or CuO are identified. XRD patterns of calcined powders (Fig. 2a) showed that the pure phase of CCTO is obtained at 1000 °C for 24 h by the solid route. Fortunately, for powders prepared by glycine, citrate and especially by the urea method the temperature and the time of calcination are much lower.

The X-ray diffraction patterns of the samples synthesized sintered at 1100 °C for 12 h are shown in Fig. 2b.

Table 1 Structural data obtained from the rietveld refinement of CCTO prepared with different methods

Synthesis method	Citrate	Solid	Urea	Glycine
Lattice parameter (A°)	7.396	7.395	7.401	7.392
Unit cell volume (A°³)	404.6	404.5	405	403.8
Density	87%	96%	91%	82%
Argument indices				
R_{exp} (%)	2.12	1.56	4.43	1.84
R_{wp} (%)	3.44	2.71	5.06	5.31
χ^2	2.8	3.2	2.68	2.9
R_{Bragg}	2.47	2.68	3.70	1.37

Table 2 The dielectric and electrical parameters at 1 kHz and RT

Synthesis method	Citrate	Solid	Urea	Glycine
ε' ($\times 10^4$)	6.735	2.674	2.027	2.130
$\tan\delta$	0.07	0.1	0.09	0.08
R_{gb} (Ω) ($\times 10^5$)	18.9	6.55	9.57	11
R_g (Ω)	20.5	501.2	3810.7	905.5

A single CCTO phase was obtained only for the sample prepared by solid state reaction. Whereas, the diffraction patterns obtained for citrate, glycine and urea samples (Fig. 2) revealed the existence of minor secondary phases attributed to the CuO or/and CaTiO₃. As can be seen, all main diffraction peaks were indexed to a body-centered cubic CCTO of space group **Im** $\overline{3}$ (No. 204), CCTO based on the Powder Diffraction File data (PDF #75–2188).

To elaborate pure phases by citrate and urea methods, we have chosen to lower the temperature and the time of the sintering. Figure 2c depicts the X-ray diffraction patterns of CCTO compounds prepared by citrate and urea methods and sintered at different thermal treatment. Comparing patterns with those of the standard powder XRD pattern of CCTO phase, obviously those obtained after calcination, the presence of CCTO was confirmed in both the samples, as a major phase. The diffractograms confirm also the disappearance of the secondary phases detected during the thermal treatment. We note just the presence only of CuO in the form of a trace in samples prepared by citrate and sintered at 1050 °C for 3 h. It is also noted that the peaks of this secondary phase disappear with the increase in sintering time or temperature. Concerning the pellets prepared

Fig. 3 Profile fits for the Rietveld refinement of CCTO ceramics prepared by citrate (**a**), solid (**b**), urea (**c**) and glycine (**d**) methods sintered at 1100 °C for 12 h
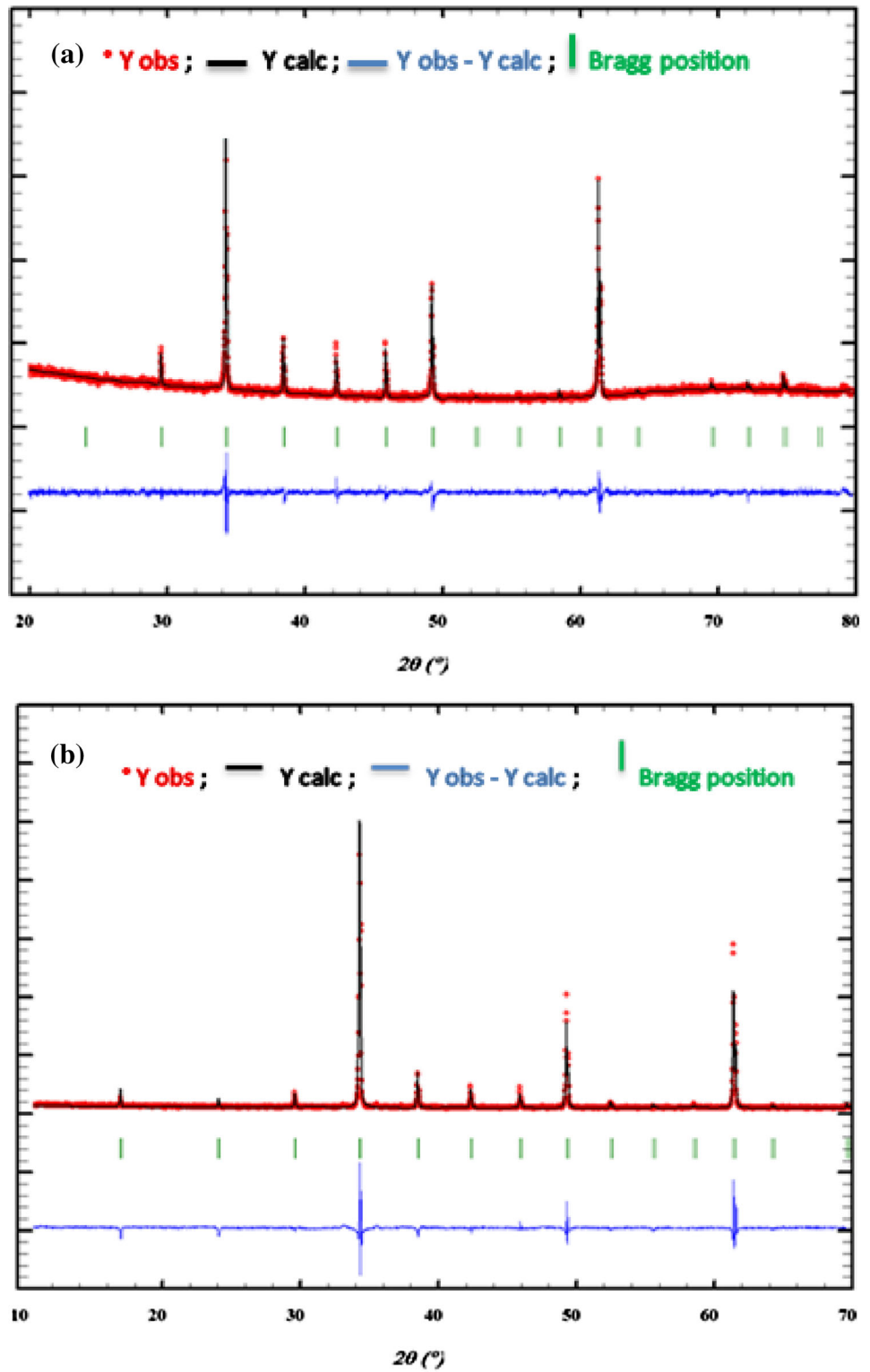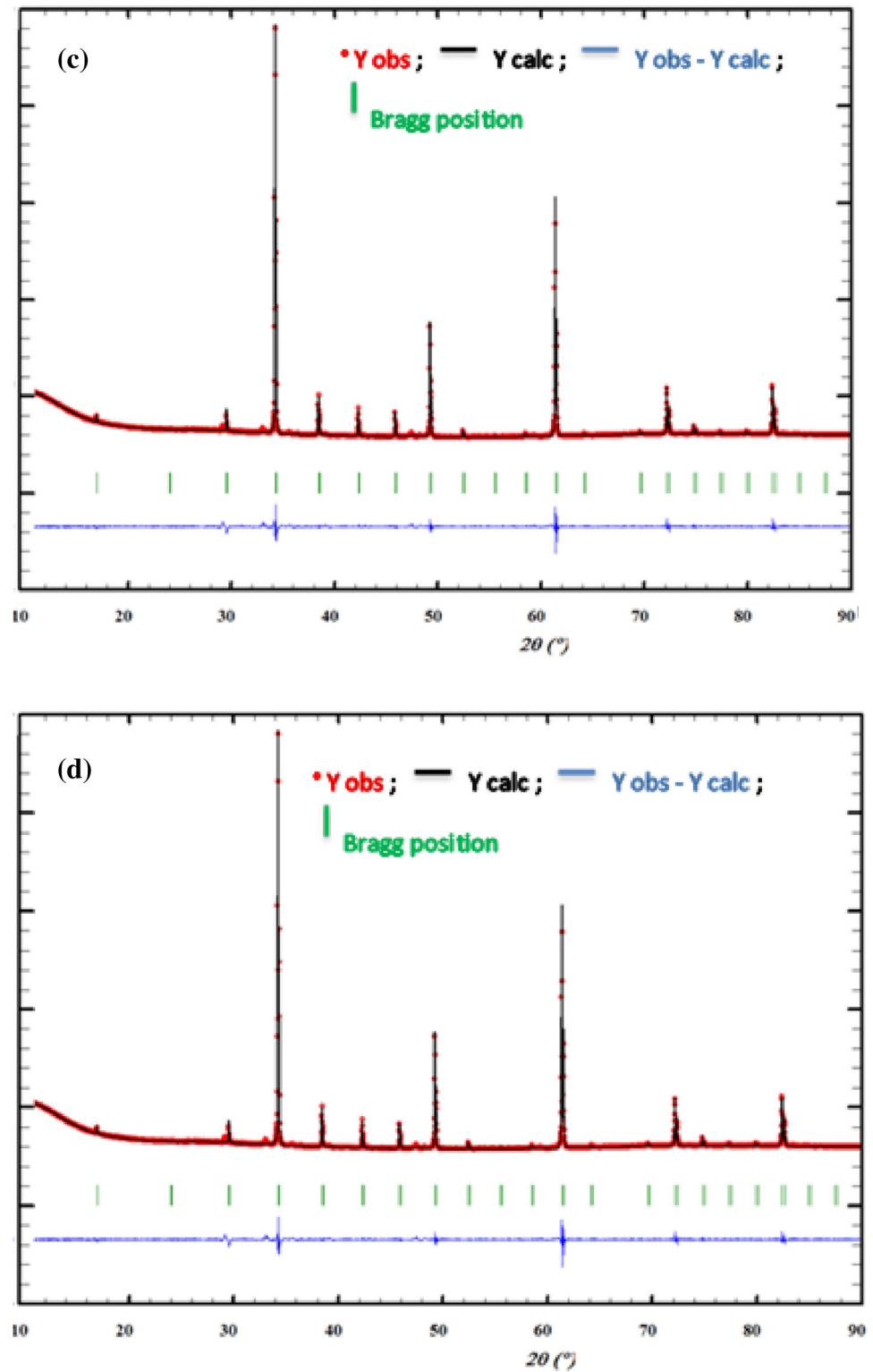
Fig. 3 continued

by urea routes, we succeeded in the synthesis of pure phase even for sintering for 3 h at 1050 °C.

Fig. 3 Illustrates Rietveld refinement of X-ray patterns diffractions of CCTO ceramics sintered at 1100 °C for 12 h. The fit of all samples confirms the

structure of cubic symmetry $Im\bar{3}$. The results of structural examinations (lattice parameters, unit cell volume and values of reliability factors) as tabulated in Table 1. The refined lattice parameter of CCTO, prepared by citrate, solid, urea and glycine methods, was found to be 7.396, 7.395, 7.40 and 7.394 Å, respectively. The results are similar to those obtained in the literature [46, 47]. The χ^2 values indicate that the process is in good refinement analysis with the released literature [48]

4.2 Scanning electron microscopy SEM

Synthesis methods play an important role on the microstructure and obviously on the electrical properties intrinsically linked to the microstructure in this type of compound. The surface's morphology and a representative histogram of grain size distributions of CCTO ceramics synthesized by different methods are presented in Fig. 4. There is a similar grain morphology regardless the synthesized procedure way. Microstructure of CCTO exhibits almost uniformity distributed throughout the ceramics with small grain size which does not exceed ten microns. The grain surfaces suggest the irregularly crystallographic facets CCTO grain shape. But the solid route produces a much more uniform homogeneity and clear grain boundaries than the other synthesis techniques. Nevertheless, the granulometry obtained by citric route (Fig. 4b) exhibits the largest grain size compared to other synthesis methods. Moreover, several numbers of grains grow abnormally, and the size of the largest abnormal grain exceeded 15 μm. A previous study explained the bimodal grain size distribution by the stoichiometry modification with the variation of Ca or Cu content. [49, 50].

Ceramics synthesized by the solid state reaction exhibit dense microstructure. Based on the theoretical densities (4.90 g.cm^{-3} [51]), the relative density values of CCTO ceramics synthesized by the solid state reaction to a maximum value of 96%. This is certainly associated to the uniform microstructure obtained in the case of solid synthesis.

Figure 5 shows SEM micrographs carried out on the grain and the grain boundary regions. Analysis based on chemical composition confirms the formation of CCTO grain regardless of grain size and synthesis methods.

A careful analyse in the grain boundaries of sample prepared by citrate route, reveals that the region is rich in Cu, which explains the growth grains compared to the others [52]. In this case, percentage of the flat second phase seems to be lower, the XRD pattern show the presence of residues CuO phase.

In the case of liquid synthesis, the significant decrease in the density of the ceramics produced is certainly associated with the nature of the microstructure which is more heterogeneous in this case compared to the solid route.

Indeed, the CCTO ceramics obtained by citrate route represent a dense microstructure (87%) with large grains (Fig. 5). For the other samples, the grain size of urea (c) and glycine (d) are smaller as compared to citrate due to the easier complex formation and heat release, resulting in more combustion enthalpy which yields a finer grain size [53]. The average grain size of samples solid (a), citrate (b), glycine (c) and urea (d) calculated using Image J software were found to be 7.63 ± 0.2 μm; 14.65 ± 0.7 μm; 10.54 ± 0.2 μm and 10.11 ± 0.3 μm, respectively. The sample obtained by citrate show the highest average grain size compared to the other samples. This result could be correlated with the presence of the liquid phase formed during sintering, leading to the improvement of the samples densification. [54]. However, the reduction of grain sizes in glycine samples could be associated the presence of $CaTiO_3$ impurities and consequently the inhibition of the grain growth [55].

4.3 Dielectric properties

4.3.1 Dielectric analysis

In this paragraph, we analyze the dielectric properties of undoped CCTO ceramics synthesized by different methods. Figure 6 exhibits the frequency dependence of the relative dielectric constant ε′ and dielectric loss (tanδ) of CCTO at room temperature in the range of 10^2–10^7 Hz. The dielectric and electrical parameters are summarized in Table 2. First, it may be noticed that all ceramics reveal higher permittivity ε of the order of 10^4 independently of the synthesis method. Secondary, in the frequency range from 10^2 to 10^6 Hz, CCTO presents a plateau (good frequency stability) followed by a rapid decrease in the high frequency. According to bibliography, the high values of the dielectric constant ε at low frequency may be attributed to the creation of a Maxwell–Wagner interfacial polarization, where charge carriers are
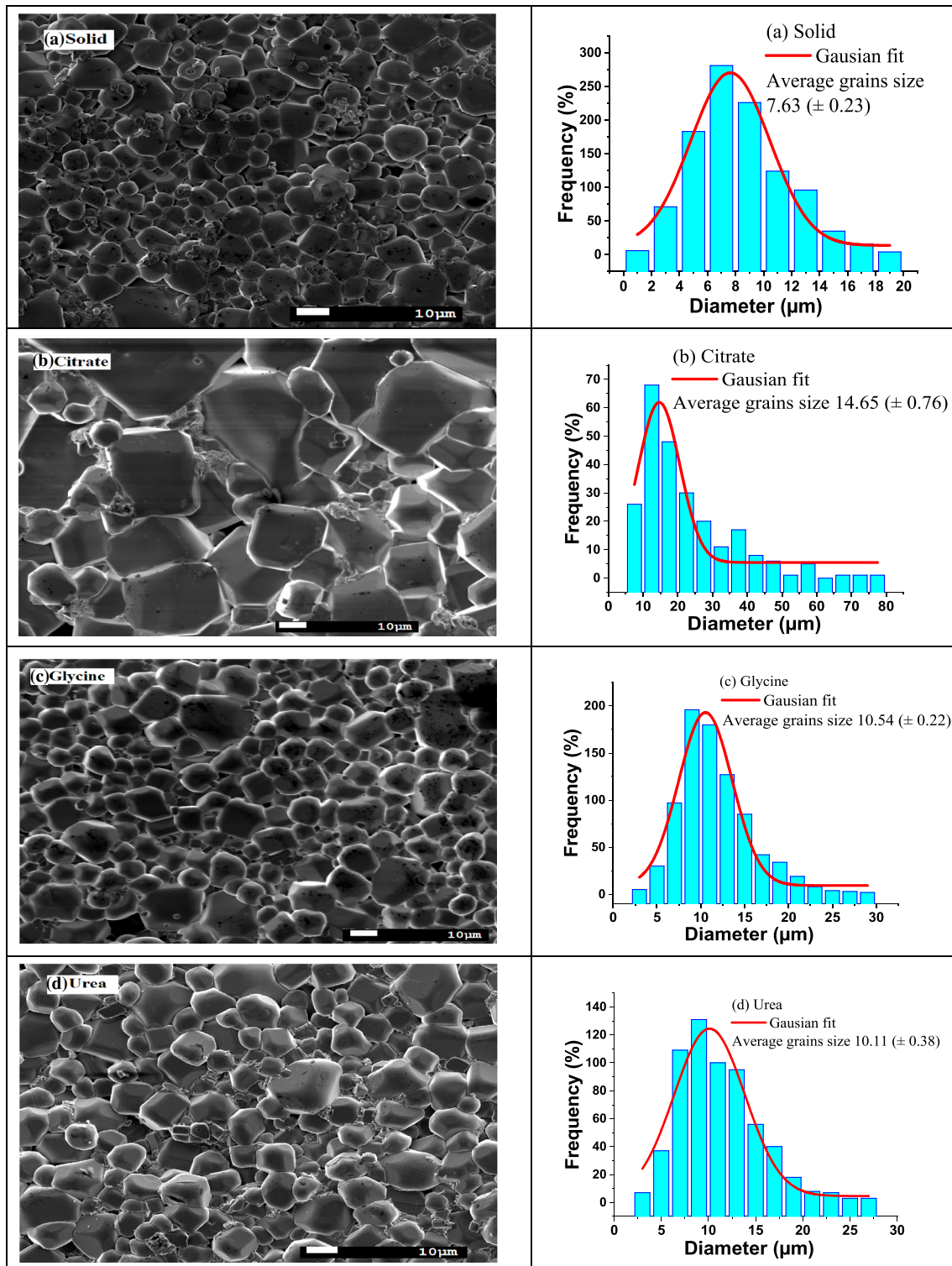
Fig. 4 SEM images of surface morphology for pure CCTO by different routes

accumulated at the interface of grain boundary and grain [56]. Moreover the phenomenon, up to 10^6 Hz, was explained by a Debye- like dipolar relaxation process [57].
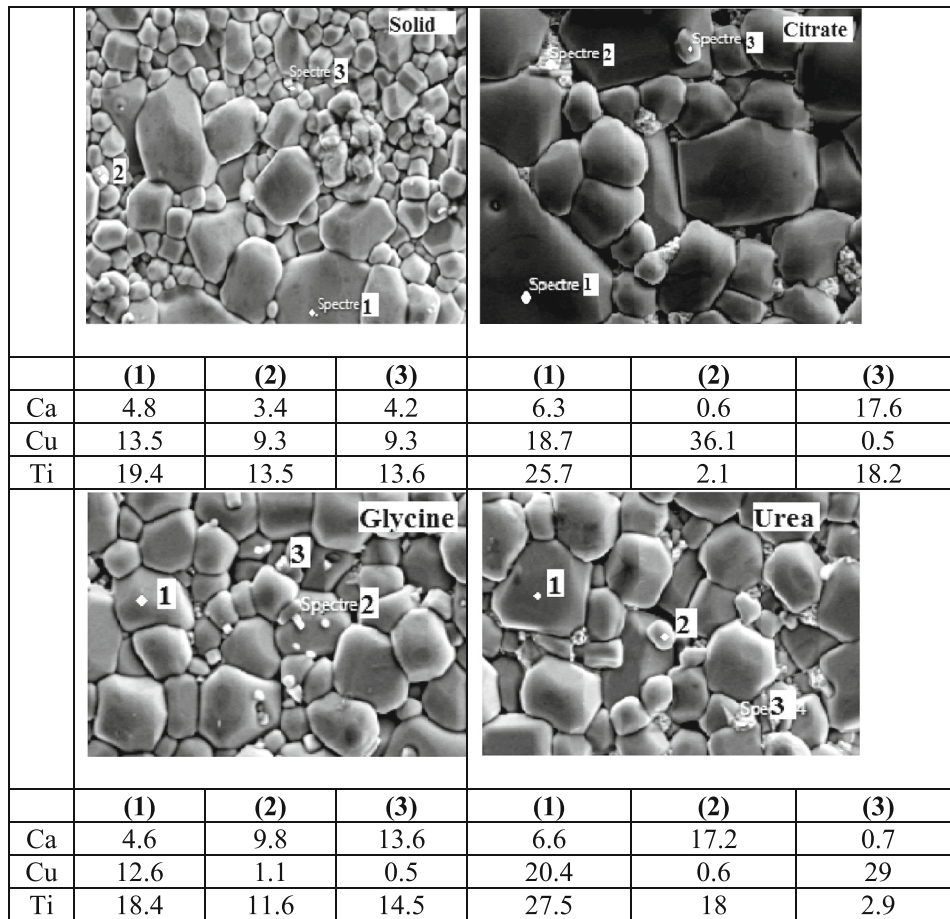
	(1)	(2)	(3)	(1)	(2)	(3)
Ca	4.8	3.4	4.2	6.3	0.6	17.6
Cu	13.5	9.3	9.3	18.7	36.1	0.5
Ti	19.4	13.5	13.6	25.7	2.1	18.2

	(1)	(2)	(3)	(1)	(2)	(3)
Ca	4.6	9.8	13.6	6.6	17.2	0.7
Cu	12.6	1.1	0.5	20.4	0.6	29
Ti	18.4	11.6	14.5	27.5	18	2.9

Fig. 5 Representative EDS detected on the surface of CCTO synthesized by diverse routes

As shown in Fig. 6, the dielectric behavior of CCTO ceramics prepared by urea and glycine is very similar, which can be explicated to their similar microstructures (mean particle size). Particularly, the considerable high dielectric constant ε' of the sample fabricated by citrate method emanates from the larger grain size as based on the IBLC model that the relative permittivity value strongly depends on the grain size (see Fig. 3).

On the other hand, as the measuring frequency increases to 10^6 Hz, the frequency-stability of permittivity decreases slightly in the CCTO ceramic obtained by citrate method. It may be due probably to the changes of microstructure and to appearance of more oxygen vacancies at high sintering temperature [58]. Moreover, this decrease in the stability domain can be explained by the dipoles starting to lag the electric field, which leads to Maxwell–Wagner relaxation behaviorin the material [59].

The frequency dependence of dielectric loss (tanδ) of the CCTO ceramics measured at room temperature is shown in Fig. 6 Fig. 6. It is clearly, independently of synthesis methods, all samples exhibit relatively neighboring and lower interesting dielectric loss ($\sim$ 0.07). It drops as frequency increases until the formation of a plateau. Then, increases again at high frequency.

Precisely, the sample obtained by citrate route reaches a value of 0.07 which is the lowest value for frequencies up 10 kHz and high dielectric constant due to the large grains improved by the presence of CuO [60, 61]. These interesting result, lower dielectric and simultaneously a high dielectric constant, can obtained if CCTO is prepared by citrate methods ant treated in condition cited before (Fig. 7).

In a low-frequency range, resistivity is nearly constant, it is of the order of 10^7–10^9 Hz. Nevertheless, as the frequency increase the resistivity was

Fig. 6 The variation of dielectric constant (**a**) and dielectric loss (**b**) versus frequency for CCTO ceramics with different methods at room temperature
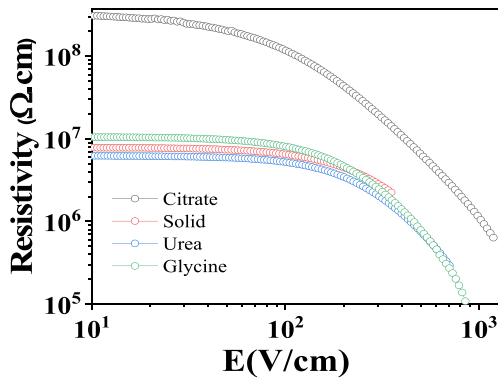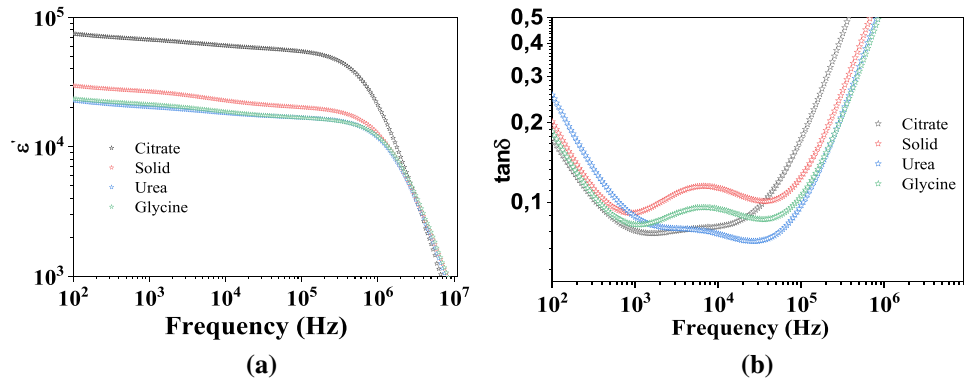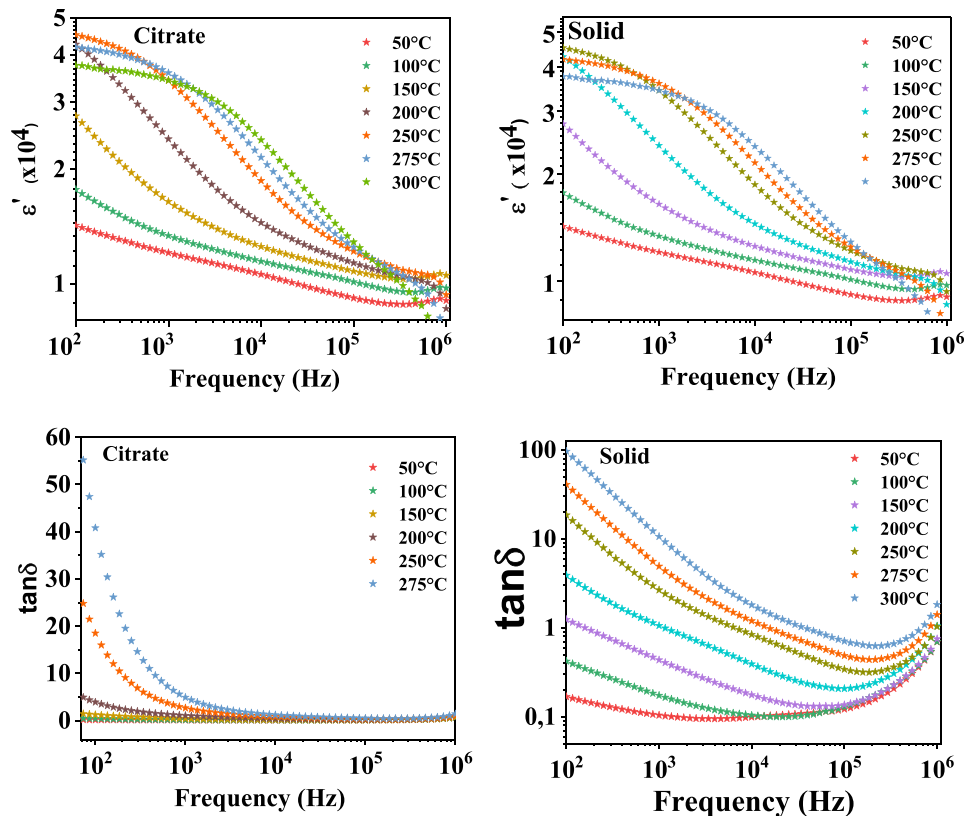

Fig. 7 The variation of resistivity as function of frequency

greatly decreased. This is in agreement with the result of dielectric loss. It is well remarkable the highest low-frequency dielectric loss is accompanied by the lowest resistivity. According to literature [62], it was found that dielectric loss of CCTO ceramics has a close relationship to their leakage current.

Figure 8 displays the frequency dependence of ε' and tanδ diferent temperatures (from 60 to 300 °C) for the CCTO ceramic sintered by citrate and solid methods. Figure 8, shows that in the low temperature, ε' depends slightly on frequency over the range from 10^2 to 10^5 Hz. However, when the temperature

Fig. 8 Frequency dependence of dielectric constant ε' and dielectric loss (tanδ) at different temperatures

is higher than 100 °C, ε' increases with increasing temperature, and strongly depends on frequency, especially in low-frequency range. Moreover, independently of all temperature ranges, dielectric constant decrease as the frequency increase. As reported in litterature, high values of obtained at low frequency can be attributed to interfacial polarization witch appears at the grain boundaries and grain. [63].

Similar trend is observed in tanδ, as shown in Fig. 8. As we can see the variation of dielectric loss was higher at low frequencies, up to 10^3 Hz, and then remains nearly constant from the frequency range of of 10^3 Hz to 10^6 Hz. As we increase the temperature, the dielectric loss also increases. At lower frequency, the high value explained by the important energy necessary to move the charge carriers accumulated at grain boundaries. In higher frequency, a lower energy able to move the charge carriers owing to the low resistance of the material [64].We conclude that the frequency and temperature effect on the dielectric loss highlights the interfacial polarization of the grain boundaries within the ceramic in the low-frequency region [65].

4.3.2 Impedance analysis

The impedance spectroscopy technique is used to examine and study the electrical responses of the material. It is based on determining the complex impedance Z* witch is decomposed into a real (Z′) and imaginary (Z″) part expressed as follows: Z*=Z′−jZ″.

The complex impedance provides some information about the electrical response inside grains and grain boundaries and about the interface effects existing in the material.

In polycrystalline ceramics, there are three possible contributions to the total observed resistance and capacitance, emanating from grains (bulk), grain boundaries (GB) and electrode specimen interface.

Figure 9 shows the Z″ vs. Z′ plots for all ceramic samples at room temperature performed in the frequency range between 100 and 10^7 Hz. This curve allows the separation of the contribution of grain and grain boundary resistance existing in the material [66]. The characterization of these parameters using Z view software. In this study can be used equivalent circuit composed by two parallel resistor–capacitor (RC) elements connected in series. According to the impedance spectroscopy analysis, it is possible to reach the values of resistivity of the grain boundaries R_{gb} and the grain R_g and for each sample. The grain boundary resistance R_{gb} can be determined by the diameter of a large semicircular arc on the impedance complex plane and the other one corresponds to the resistance of grains R_g can be obtained at high frequency from the non-zero intercept on Z′ axis at high frequency [67–69].

The fitted parameters values were reported in Table 1.The R_{gb} and R_g values change considerably according to the synthesis route. It can be also noted that the values of R_{gb} are significantly higher than those of R_g. These results revealed that the response corresponds to the grain boundaries effect while the response of the grain is negligible [70].

One can also note that the variation in tan δ which can be confirmed by the enhancement of R_{gb}. (tan $\delta = \frac{1}{wR_{gb}C_p}$, where R_{gb} represents the resistance of insulating Gbs, w is the angular frequency and C_P is the capacitance of the sample). The citrate sample shows the highest R_{gb} value 1.89×10^6 [71, 72], leading to the lower loss compared to the other sample. This electrical response is related to the Gbs behave such as an insulating grain and the grains as semiconducting in CCTO ceramics, which is in agreement with the IBLC model [73].

Fig. 9 The plots of the real part of impedance Z′ as a function of its imaginary part Z″ at room temperature of CCTO pellets synthesized by different methods. The inset shows a non-zero intercept with the Z axis
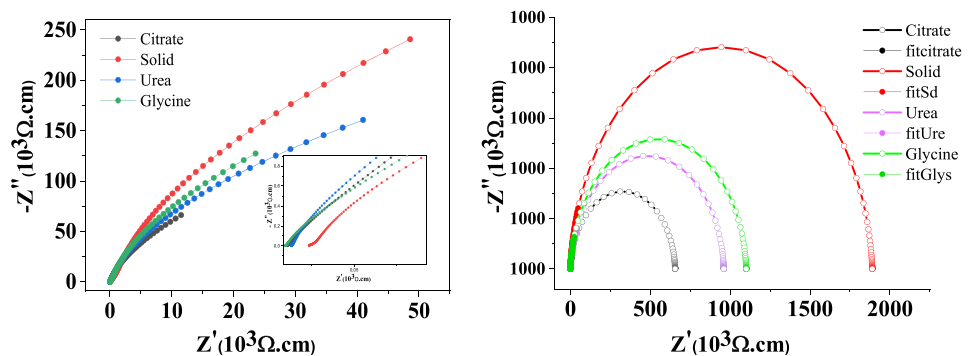
5 Conclusions

$CaCu_3Ti_4O_{12}$ powders were successfully synthesized by different methods, namely, solid state, citrate method, semi-wet route using glycine and semi-wet route using urea. As expected, $CaCu_3Ti_4O_{12}$ is an excellent material with good dielectric properties and was successfully synthesized by citrate method. The results of X-ray diffraction showed the formation of single phase CCTO compared to the other process which revealed the existence of secondary phases attributed to the $CaTiO_3$ and CuO. The SEM images indicate clearly the presence of abnormal grain growth. Although the average grain sizes were different, the CCTO obtained by citrate show the highest average grain size compared to the other samples. The dielectric property of ceramic samples was found to have high dielectric constants allows 10^4.

Combining the ε' results with the SEM images, the dielectric properties of the CCTO ceramics are associated with an internal barrier layer capacitor (IBLC) model. High-dielectric constant ε' (6.735×10^4) and low-tanδ (0.07) were achieved in the sample citrate method. The lowest tanδ value in this sample was associated with the highest R_{gb} (1.89×10^6 Ω).

Author Contributions

All authors contributed to the study conception and design. Material preparation, data collection and analysis were performed by ES, SS and DN, the material used is made available by the team of CA and AM. The first version of the manuscript was written by ES and SS and all authors have commented on previous versions of the manuscript.

Data Availability

The datasets generated during and/or analysed during the current study are available from the corresponding author on reasonable request.

Declarations

Conflict of interest The authors have no relevant financial or non-financial interests to disclose. Conflict of interest: The authors declare that they have no conflict of interest.

Ethical approval All authors have read and agreed to the published version of the manuscript.

References

1. G. Du, F. Wei, W. Li, N. Chen, Co-doping effects of A-site Y^{3+} and B-site Al^{3+} on the microstructures and dielectric properties of $CaCu_3Ti_4O_{12}$ ceramics. J Eur. Ceram. Soc. **37**, 4653–4659 (2017)
2. X. Huang, H. Zhang, Y. Lai, J. Li, The lowered dielectric loss tangent and grain boundary effects in fluorine-doped calcium copper titanate ceramics. Appl. Phys. A. **123**, 317 (2017)
3. L. Ni, X.M. Chen, Enhancement of giant dielectric response in $CaCu_3Ti_4O_{12}$ Ceramics by Zn Substitution. J. Am. Ceramic. Soc. **93**, 184–189 (2010)
4. M.A. Subramanian, D. Li, N. Duan, B.A. Reisner, A.W. Sleight, High dielectric constants in $ACu_3Ti_4O_{12}$ and $ACu_3Ti_3FeO_{12}$. J. Solid State Chem. **151**, 323–325 (2000)
5. C.C. Homes, T. Vogt, S.M. Shapiro, S. Wakimoto, A.P. Ramirez, Optical response of high-dielectric-constant perovskite-related oxide. Science **293**, 673 (2001)
6. S.-Y. Chung, I.-D. Kim, S.-J.L. Kang, Strong nonlinear current–voltage behaviour in perovskite-derivative calcium copper titanate. Nat. Mater. **3**, 774–778 (2004)
7. S. Kaur, A. Kumar, A.L. Sharma, D.P. Singh, Dielectric and energy storage behavior of $CaCu_3Ti_4O_{12}$ nanoparticles for capacitor application. Ceram. Int **45**, 7743–7747 (2019)
8. R. Schmidt, D.C. Sinclair, $CaCu_3Ti_4O_{12}$ (CCTO) ceramics for capacitor applications. RSC Adv. **3**, 1402–1621 (2014)

9. L.C. Kretly, A.F.L. Almeida, R.S. de Oliveira, J.M. Sasaki, A.S.B. Sombra, Electrical and optical optical properties of $CaCu_3Ti_4O_{12}$ (CCTO) substrates for microwave devices and antennas. Microw. Opt. Technol. Lett. **39**, 145–150 (2003)

10. M. Li, X.L. Chen, D.F. Zhang, W.Y. Wang, W.J. Wang, Humidity sensitive properties of pure and Mg-doped $CaCu_3Ti_4O_{12}$. Sens. Actuators B: Chem. **147**, 447–452 (2010)

11. A. Natkaeo, D. Phokharatkul, J.H. Hodak, A. Wisitsoraat, S.K. HodakNatkaeo, Highly selective Sub–10 Ppm H2S gas sensors based on Ag-Doped CaCu3Ti4O12 films. Sens. Actuators B: Chem. **260**, 571–580 (2018)

12. H. Yu, H. Liu, D. Luo, M. Cao, Microwave synthesis of high dielectric constant $CaCu_3Ti_4O_{12}$. J. Mater. Process. Technol. **208**, 145–148 (2008)

13. W. Li, L. Tang, F. Xue, Z. Xin, Z. Luo, G. Du, Large reduction of dielectric losses of $CaCu_3Ti_4O_{12}$ ceramics via air quenching. Ceram. Int. **43**, 6618–6621 (2017)

14. A. Smith, T. Calvarese, A. Sleight, M. Subramanian, An anion substitution route to lo loss colossal dielectric $CaCu_3Ti_4O_{12}$. J. Solid State Chem. **182**, 409–411 (2009)

15. M.H. Cohen, J.B. Neaton, L. He, D. Vanderbilt, Extrinsic models for the dielectric response of $CaCu_3Ti_4O_{12}$. J. Appl. Phys. **94**, 3299 (2003)

16. P. Lunkenheimer, R. Fichtl, S.G. Ebbinghaus, A. Loidl, Non-intrinsic origin of the colossal dielectric constants in $CaCu_3Ti_4O_{12}$. Phys. Rev. **70**, 172102 (2004)

17. S. Krohns, P. Lunkenheimer, S.G. Ebbinghaus, A. Loidl,Broadband dielectric spectroscopy on single-crystalline and ceramic $CaCu_3Ti_4O_{12}$.Appl. Phys. Lett. **91**, 022910 (2007)

18. P.R. Bueno, R. Tararan, R. Parra, E. Joanni, M.A. Ramírez, W.C. Ribeiro, E. Longo, J.A. Varela, A polaronic stacking fault defect model for $CaCu_3Ti_4O_{12}$ material: an approach for the origin of the huge dielectric constant and semiconducting coexistent features. J. Phys. D: Appl. Phys. **42**, 055404 (2009)

19. W.C. Ribeiro, E. Joanni, R. Savu, P.R. Bueno, Nanoscale effects and polaronic relaxation in $CaCu_3Ti_4O_{12}$ compounds. Solid State Commun. **151**, 173–176 (2011)

20. D.C. Sinclair, T.B. Adams, F.D. Morrison, A.R. West, $CaCu_3Ti_4O_{12}$: one-step internal barrier layer capacitor. Appl. Phys. Lett. **80**, 2153–2155 (2002)

21. R. Schmidt, M.C. Stennett, N.C. Hyatt, J. Pokorny, J. Prado-Gonjal, M. Li, D.C. Sinclair, Effects of sintering temperature on the internal barrier layer capacitor (IBLC) structure in $CaCu_3Ti_4O_{12}$ (CCTO) ceramics. J. Eur. Ceram. Soc. **32**, 3313–3323 (2012)

22. J. Jumpatam, B. Putasaeng, N. Chanlek, P. Kidkhunthod, P. Thongbai, S. Maensiri, P. Chindaprasirt, Improved giant dielectric properties of $CaCu_3Ti_4O_{12}$ via simultaneously tuning the electrical properties of grains and grain boundaries by F^- substitution. RSC Adv. **7**, 4092–4101 (2017)

23. M.J. Abu, J.J. Mohamed, M.F. Ain, Z.A. Ahmad, Phase structure, microstructure and broadband dielectric response of Cu nonstoichiometry $CaCu_3Ti_4O_{12}$ ceramic. J. Alloys Compd. **683**, 579–589 (2016)

24. A. Onodera, K. Kawatani, M. Takesada, M. Oda, M. Ido, Dielectric and thermal properties of single-crystalline $CaCu_3Ti_4O_{12}$ at high temperatures. J. Appl. Phys. **48**, 09KF12 (2009)

25. X.W. Wang, P.B. Jia, X.E. Wang, B.H. Zhang, L.Y. Sun, Q.B. Liu, Calcining temperature dependence on structure and dielectric properties of CaCu3Ti4O12 ceramics. J. Mater. Sci.: Mater Electron. **27**, 12134–12140 (2016)

26. Y. Qiu, Z.J. Zou, L.H. Zhou, M.R. Bai, X.H. Li, Microstructure, dielectric and nonlinear electrical properties associated with sintering conditions in calcium copper titanate ceramics. J. Mater. Sci.: Mater Electron. **28**, 11091–11097 (2017)

27. T.C. Porfirio, E.N.S. Muccillo, Dielectric properties of $CaCu_3Ti_4O_{12}$ synthesized by different routes. J. Adv. Mater. Res. **975**, 184–188 (2014)

28. W. Hao, J. Zhang, Microstructure and dielectric property of hot-pressed high density $CaCu_3Ti_4O_{12}$ ceramics. J. Alloys Compd. **559**, 16–19 (2013)

29. S. Saîd, S. Didry, M. El Amrani, C. Autret-Lambert, A. Megriche, Brilliant effect of Ni substitution in the appearance of high dielectric constant in $CaCu_{2.9}Ni_{0.1}Ti_{3.9}Ni_{0.1}O_{12}$ Ceramics. J. Alloys Compd. **765**, 927–935 (2018)

30. V.S. Puli, S. Adireddy, M. Kothakonda, R. Elupula, D.B. Chrisey, Low temperature sintered giant dielectric constant $CaCu_3Ti_4O_{12}$ sol-gel synthesized nanopartic capacitors. J. Adv. Dielectr. **7**, 1750017 (2017)

31. J. Liu, Y. Sui, C.-G. Duan, W.-N. Mei, R.W. Smith, J.R. Hardy, $CaCu_3Ti_4O_{12}$: Low- temperature synthesis by pyrolysis of an organic solution. Chem. Mater. **18**, 378–3882 (2006)

32. B. Zhu, Z. Wang, Y. Zhang, Z. Yu, J. Shi, R. Xiong, Low temperature fabrication of the giant dielectric material $CaCu_3Ti_4O_{12}$ by oxalate coprecipitation method. Mater. Chem. Phys. **113**, 746–748 (2009)

33. A.K. Rai, K.D. Mandal, D. Kumar, O. Parkash, Characterization of nickel doped CCTO: $CaCu_{2.9}Ni_{0.1}Ti_4O_{12}$ and $CaCu_3Ti_{3.9}Ni_{0.1}O_{12}$ synthesized by semi-wet route. J. Alloys Compd. **491**, 507–512 (2010)

34. J. Jumpatam, P. Thongbai, Enhanced dielectric and non-ohmic properties in $CCTO/CaTiO_3$ nanocomposites prepared by a chemical combustion method. J. Mater. Sci.: Mater Electron. **27**, 12085–12090 (2016)

35. K. Pal, R. Jana, A. Dey, P.P. Ray, M.M. Seikh, A. Gayen, Application of CaCu$_3$Ti$_4$O$_{12}$ based quadruple perovskites as a promising candidate for optoelectronic devices. Chem. Phys. Lett. **699**, 229–233 (2018)

36. L. Singh, I.W. Kim, W.S. Woo, B.C. Sin, H.-I. Lee, Y. Lee, A novel low cost non-aqueous chemical route for giant dielectric constant CaCu$_3$Ti$_4$O$_{12}$ Ceramic. Solid State Sci. **43**, 35–45 (2015)

37. P. Mao, J. Wang, S. Liu, L. Zhang, Y. Zhao, L. He, Grain size effect on the dielectric and non-ohmic properties of CaCu$_3$Ti$_4$O$_{12}$ ceramics prepared by the sol-gel process. J. Alloys Compd. **778**, 625–632 (2019)

38. P. Thongbai, T. Yamwong, S. Maensiri, V. Amornkitbamrung, P. Chindaprasirt, Improved dielectric and nonlinear electrical properties of fine-Grained CaCu$_3$Ti$_4$O$_{12}$ ceramics prepared by a glycine-nitrate process. J. Am. Ceram. Soc. **97**, 1785–1790 (2014)

39. D. Gingaşu, L. Patron, N. Stanica, I. Balint, Rev. Roum. Chim. **49**, 669–674 (2004)

40. F. Amaral, M. Valente, L. Costa, Synthesis and characterization of calcium copper titanate obtained by ethylenediaminetetraacetic acid gel combustion. Mater. Chem. Phys. **124**, 580–586 (2010)

41. A. Douy, Polyacrylamide gel: an efficient tool for easy synthesis of multicomponent oxide precursors of ceramics and glasses. J. Inorg. Mater. **3**, 699–707 (2001)

42. V. Brizé, G. Gruener, J. Wolfman, K. Fatyeyeva, M. Tabellout, M. Gervais, F. Gervais, Grain size effects on the dielectric constant of CaCu$_3$Ti$_4$O$_{12}$ ceramics. J. Mater. Sci. Eng. B. **129**, 135–138 (2006)

43. S. De Almeida-Didry, C. Autret, C. Honstettre, A. Lucas, F. Pacreau, F. Gervais, Capacitance scaling of grain boundaries with colossal permittivity of CaCu$_3$Ti$_4$O$_{12}$ -based materials. Solid State Sci. **42**, 25–29 (2015)

44. J. Rodríguez-Carvajal, Recent advances in magnetic structure determination by neutronpowder diffraction. Phys. B:Condens. Matter. **192**, 55–69 (1993)

45. X.W. Wang, P.B. Jia, X.E. Wang, B.H. Zhang, L.Y. Sun, Q.B. Liu, Electron. **27**, 12134–12140 (2016)

46. J. Li, A.W. Sleight, M.A. Subramanian, Evidence for internal resistive barriers in a crystal of the giant dielectric constant material: CaCu$_3$Ti$_4$O$_{12}$. Solid State Commun. **135**, 260–262 (2005)

47. W. Li, Lu. Tang, F. Xue, Z. Xin, Z. Luo, Du. Guoping, Large reduction of dielectric losses of CaCu$_3$Ti$_4$O$_{12}$ ceramics via air quenching. Ceram. Int. **43**, 6618–6621 (2017)

48. S. Nasri, A.L. Ben Hafsia, M. Tabellout, M. Megdiche, Complex impedance, dielectric properties and electrical conduction mechanism of La$_{0.5}$Ba$_{0.5}$FeO$_{3-\delta}$ perovskite oxides. RSC Adv. **6**, 76659–76665 (2016)

49. D.-L. Sun, A.-Y. Wu, S.-T. Yin, Structure, properties, and impedance spectroscopy of CaCu$_3$Ti$_4$O$_{12}$ ceramics prepared by sol-gel process. J. Am. Ceramic. Soc. **91**, 169–173 (2008)

50. M. Abu, M. Rahman, R. Zaman, M. Ahmadipour, J. Mohamed, M.F. Ain, Z. Ahmad, Microwave dielectric properties of Ca1+XCu3Ti4O12+X ($-0.04 \leq X \leq 0.04$) Ceramics. Procedia Chem. **19**, 929–934 (2016)

51. T.T. Fang, C.P. Liu, Evidence of internal domains for inducing the anomalously high dielectric constant of CaCu$_3$Ti$_4$O$_{12}$. Chem. Mater. **17**, 5167–5171 (2005)

52. L. Singh, U.S. Rai, K.D. Mandal, A.K. Rai, Effect of processing routes on microstructure, electrical and dielectric behavior of Mg-Doped CaCu$_3$Ti$_4$O$_{12}$ electro-ceramic. Appl. Phys. A. **112**, 891–900 (2013)

53. J. Mohamed, S.D. Hutagalung, Z.A. Ahmad, Influence of Sintering Parameters on Melting Cuo Phase in CaCu$_3$Ti$_4$O$_{12}$. J. King Saud Univ. Eng. Sci. **25**, 35–39 (2013)

54. K.M. Kim, J.H. Lee, K.M. Lee, D.Y. Kim, D.H. Riu, S.B. Lee, Microstructural evolution and dielectric properties of Cu-deficient and Cu-excess CaCu$_3$Ti$_4$O$_{12}$ ceramics. Mater. Res. Bull. **43**, 284–291 (2008)

55. Y. Guo, J. Tan, J. Zhao, Influence of CTO additives on microstructure and electrical properties of CCTO ceramics. Mater. Chem. Phys. **278**, 125659 (2022)

56. Z. Xu, H. Qiang, Y. Chen, Z. Chen, Microstructure and enhanced dielectric properties of yttrium and zirconium co-doped CaCu$_3$Ti$_4$O$_{12}$ ceramics. Mater. Chem. Phys. **191**, 1–5 (2017)

57. S. Ke, P. Lin, H. Huang, H. Fan, X. Zeng, Mean-field approach to dielectric relaxation in giant dielectric constant perovskite ceramics. J. Ceram. **2013**, 1–7 (2013)

58. S. Su, R. Zuo, Y. Ran, W. Zhao, X. Wang, L. Li, Microstructure, electrical properties and processing dependence of CuO modified (Na$_{0.52}$K$_{0.48}$)NbO3 ceramics. Ceram. - Silik. **54**, 320–324 (2010)

59. S. Sil, J. Datta, M. Das, R. Jana, S. Halder, A. Biswas, D. Sanyal, P.P. Ray, Bias dependent conduction and relaxation mechanism study of Cu$_5$FeS$_4$ film and its significance in signal transport network. J. Mater. Sci. **29**, 5014–5024 (2018)

60. M. Li, G. Cai, D.F. Zhang, W.Y. Wang, W.J. Wang, X.L. Chen, Enhanced dielectric responses in Mg-doped CaCu$_3$Ti$_4$O$_{12}$. J. Appl. Phys. **104**, 074107 (2008)

61. FengChao Luo, JinLiang He, Hu. Jun, YuanHua Lin, Characterization of individual grain boundaries and grains of CaCu$_3$Ti$_4$O$_{12}$ ceramic. Sci. China Technol. Sci. **55**, 879–882 (2012)

62. D. Singh, Y. Mohapatra, D. Agrawal, Dielectric and leakage current properties of sol-gel erived calcium copper titanate CaCu$_3$Ti$_4$O$_{12}$ thin films and CCTO/ZrO$_2$ multilayers Mater. Sci. Eng. B. **157**, 58–65 (2009)

63. L. Singh, U.S. Rai, K.D. Mandal, B.C. Sin, H. Lee, H. Chung, Y. Lee, Comparative dielectric studies of nanostructured $BaTiO_3$, $CaCu_3Ti_4O_{12}$ and $0.5BaTiO_3 \cdot 0.5 CaCu_3Ti_4O_{12}$ nano-composites synthesized by modified sol–gel and solid state methods. Mater. Charac. **96**, 54–62 (2014)

64. K. Parida, R.N.P. Choudhary, Structural, electrical, optical and magneto-electric characteristics of chemically synthesized $CaCu_3Ti_4O_{12}$ dielectric ceramics. Mater. Res. Express. **4**, 076302 (2017)

65. J. Boonlakhorn, P. Kidkhunthod, P. Thongbai, A novel low cost non-aqueous chemical route for giant dielectric constant $CaCu_3Ti_4O_{12}$ ceramic. J. Eur. Ceram. Soc. **35**, 3521–3528 (2015)

66. G. Riquet, S. Marinel, Y. Breard, C. Harnois, A. Pautrat, Direct and hybrid microwave solid state synthesis of $CaCu_3Ti_4O_{12}$ ceramic: microstructures and dielectric properties. Ceram. Int **44**, 15228–15235 (2018)

67. J. Boonlakhorn, N. Chanlek, J. Manyam, P. Srepusharawoot, S. Krongsuk, P. Thongbai, Enhanced giant dielectric properties and improved nonlinear electrical response in acceptor−donor (Al^{3+}, Ta^{5+})-substituted $CaCu_3Ti_4O_{12}$ ceramics. J. Adv. Ceram. **10**, 1243–1255 (2021)

68. P. Mao, J. Wang, L. Zhang, Z. Wang, F. Kang, S. Liu, D.B.K. Lim, X. Wang, H. Gong, Significantly enhanced breakdown field with high grain boundary resistance and dielectric response in $0.1Na_{0.5}Bi_{0.5}TiO_3$-$0.9BaTiO_3$ doped $CaCu_3Ti_4O_{12}$ ceramics. J. Eur. Ceram. Soc. **40**, 3011–3018 (2020)

69. C. Zhao, J. Wu, Effects of secondary phases on the high-performance colossal permittivity in titanium dioxide ceramics. ACS Appl. Mater. Interfaces. **10**, 3680–3688 (2018)

70. A. Sakthisabarimoorthi, S.A. Martin Britto Dhas, R. Robert, M. Jose, Influence of erbium doping on the electrical behaviour of $CaCu_3Ti_4O_{12}$ ceramics probed by impedance spectroscopy analysis. Mater. Res. Bull. **106**, 81–92 (2018)

71. S. Rhouma, A. Megriche, M. El Amrani, S. Said, S. Roger, C. Autret-Lambert, Effect of Sr/Mg co-doping on the structural, dielectric, and electrical properties of $CaCu_3Ti_4O_{12}$ ceramics. J. Mater. Sci. Mater. Electron. **33**, 4535–4549 (2022)

72. S. Rhouma, S. Saîd, C. Autret, S. De Almeida-Didry, M. El Amrani, A. Megriche, Comparative studies of pure, Sr-doped, Ni-doped and co-doped $CaCu_3Ti_4O_{12}$ ceramics: Enhancement of dielectric properties. J. Alloys Compd. **717**, 121–126 (2017)

73. J.L. Li, F. Li, Y.Y. Zhuang, L. Jin, L.H. Wang, X.Y. Wei, Z. Xu, S.J. Zhang, Microstructure and dielectric properties of (Nb +In) Co-doped rutile TiO_2 ceramics. J. Appl. Phys. **116**, 074105 (2014)